ELSEVIER

Physica B 283 (2000) 232–236

PHYSICA B

www.elsevier.com/locate/physb

X-ray scattering from freely suspended smectic films: resolution and other effects

D. Sentenac[a], A. Fera[a], R. Opitz[a], B.I. Ostrovskii[b], O. Bunk[c], W.H. de Jeu[a,*]

[a]*FOM Institute for Atomic and Molecular Physics, Kruislaan 407, 1098 SJ Amsterdam, The Netherlands*
[b]*Institut of Crystallography, Academy of Science of Russia, Leninski pr. 59, Moscow 117333, Russia*
[c]*Universtität of Hamburg, Institut of Experimental Physics 2, Luruper Chaussee 149, D-22761 Hamburg, Germany*

Abstract

Off-specular X-ray diffuse scattering from a free suspended smectic film has been performed using different scanning geometries. Rocking scans and diffuse scans out of the plane of incidence are analyzed using a general formalism to describe the resolution function. The diffuse intensity is calculated via the use of Gaussian distributions for the resolution function within the framework of the first Born approximation. For each of the scanning geometries, practical analytical expressions are given which account well for the experimental data.

PACS: 61.30.Cz; 68.15. + e; 61.10.-i; 05.40. + j

Keywords: Smectic films; X-ray reflectivity; Diffuse scattering; Resolution function

1. Introduction

Diffuse X-ray scattering has developed into a key tool for the investigation of surfaces and interfaces of solid and liquid films (e.g. Refs. [1,2]). The decay of the diffuse intensity away from the specular beam gives information about the roughness correlations at interfaces and has been used in particular to characterise liquid surface capillary waves [1,3]. In practice, the decay of the diffuse scattering depends crucially on the experimental resolution. A resolution function $\mathscr{R}$ emerges from the existence of slits before and after the sample that define in combination with the geometry of the experiments the solid angles over which the scattering function S must be averaged. The general geometry of a scattering set-up is pictured in Fig. 1. The incident and scattered wave-vectors are denoted as $\boldsymbol{k}_{\mathrm{in}}$ and $\boldsymbol{k}_{\mathrm{out}}$ and define the wave-vector transfer $\boldsymbol{q} = \boldsymbol{k}_{\mathrm{out}} - \boldsymbol{k}_{\mathrm{in}}$, where $|\boldsymbol{k}| = 2\pi/\lambda$, with λ being the X-ray wavelength. In the incoherent limit as defined by Sinha et al. [4], $I(\boldsymbol{q})$ can be simply expressed as a convolution:

$$I(\boldsymbol{q}) = \int S(\boldsymbol{q} - \boldsymbol{q}')\mathscr{R}(\boldsymbol{q}')\,\mathrm{d}\boldsymbol{q}', \tag{1}$$

where $\boldsymbol{q}'$ denotes the stochastic deviation from the ideal wave-vector $\boldsymbol{q}$ and $\mathscr{R}$ describes the distribution of $\boldsymbol{q}'$. One way to avoid complications in finding the proper analytical form for $\mathscr{R}$ is to solve the resolution problem numerically. Then, S is integrated point by point over the real experimental solid angles [5]. However, in some cases the convergence of the associated integral relies on the form of S, and may not be systematically achieved. In this situation, an alternative is to use suitable analytical approximations for $\mathscr{R}$. These can be easily derived using Gaussian distributions, and have been shown to compare well with experimental data in the past. Some useful approximated relations have been reported for scattering geometries in the plane of incidence like specular reflectivity [6], rocking scans [7] and Bragg diffraction [2]. For more complicated geometries like surface diffraction [2] or diffuse scattering out of the plane of incidence [8], which require an averaging of S over a full resolution volume, recently approximations have been derived from a general form of $\mathscr{R}$ [9]. In the present paper, we show

* Corresponding author.
E-mail address: dejeu@amolf.nl (W.H. de Jeu)

0921-4526/00/$ - see front matter
PII: S0921-4526(99)01978-X

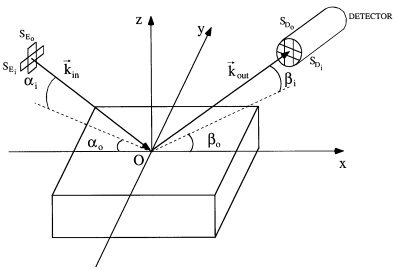

Fig. 1. General scattering geometry of a z-axis setup. The incidence plane is defined by the incident wave-vector $\boldsymbol{k}_{\mathrm{in}}$ and the surface normal (O_z).

the validity of these relations for the case of diffuse X-ray scattering from freely suspended smectic films in different scanning geometries.

2. Experimental

A freely suspended film of the liquid-crystalline compound abbreviated as 40.8 [10] was formed over a metallic frame and enclosed in a two-stage oven at $T = 63^{\circ}\mathrm{C}$ in the smectic A phase. The film was prealably studied by specular X-ray reflectivity and consisted of a stack of $N = 8$ molecular layers with a thickness $d = 28.4$ Å each, oriented parallel to the film surfaces [10].

Diffuse reflectivity measurements were performed at beamline BW2 (Hasylab, Hamburg, Germany) using a z-axis type vertical surface diffractometer (α_{i} as defined in Fig. 1 is in the horizontal plane, the sample is vertical). The principal optical elements consist of a plane premirror, a $(+/-)$ double crystal fixed-exit monochromator with two independent Si(1 1 1)-crystals set at an X-ray energy of 10.0 keV. The beam was focused sagittally by bending the second monochromator crystal and tangentially by a bent mirror in the monochromatic beam. As illustrated in Fig. 1, a rectangular cross-section of the incoming beam is defined by two orthogonal sets of slits denoted, $S_{E_{\mathrm{i}}}$ and $S_{E_{\mathrm{o}}}$, respectively, perpendicular to $\boldsymbol{k}_{\mathrm{in}}$ (pre-sample slits). The detector aperture is limited by two orthogonal sets of slits, $S_{D_{\mathrm{i}}}$ and $S_{D_{\mathrm{o}}}$, respectively, perpendicular to $\boldsymbol{k}_{\mathrm{out}}$ (detector slits). The angles α_{i} and α_{o} define the position of $\boldsymbol{k}_{\mathrm{in}}$ and the angles β_{i} and β_{o} define the position of $\boldsymbol{k}_{\mathrm{out}}$, the plane of incidence being defined by $\boldsymbol{k}_{\mathrm{in}}$ and the horizontal axis (O_z). The incident beam profiles were recorded by scanning the detector vertically (β_{o} scan) and horizontally (β_{i} scan). The profiles obtained with the slit settings listed in Table 1 are shown in Figs. 2 and 3. The recorded intensity $I(\beta_{\mathrm{i,o}})$ consist of the convolution of the intrinsic half-width at half-maximum $\mathrm{HWHM}_{\mathrm{i,o}}$ of the incident beam (assumed to be Gaussian) with the detector slits $S_{D_{\mathrm{i,o}}}$, respectively. At a distance D between the detector and the center of the diffractometer (coinciding with O in Fig. 1) it can be written as

$$I(\beta_{\mathrm{i,o}}) = I_0 \exp\left(-\frac{\beta_{\mathrm{i,o}}^2 \ln 2}{\mathrm{HWHM}_{\mathrm{i,o}}^2} \right) \Pi(\beta_{\mathrm{i,o}}), \tag{2}$$

with

$$\Pi(\beta_{\mathrm{i,o}}) = \begin{cases} 1 & \text{if } 2|\beta_{\mathrm{i,o}}| \leqslant \arctan(S_{D_{\mathrm{i,o}}}/D), \\ 0 & \text{elsewhere.} \end{cases}$$

Table 1
Resolution settings used for the different scanning geometries

Type of scan	Slit settings (mm)	Angle settings (deg)	In-plane divergence $\Delta\alpha_{\mathrm{i}}$ (mdeg)	Out-plane divergence $\Delta\alpha_{\mathrm{o}}$ (mdeg)
Rocking scan (circles)	$S_{E_{\mathrm{i}}} = 0.1$			
	$S_{E_{\mathrm{o}}} = 0.2$	$\lvert\omega\rvert \leqslant 1.2$		
		$\alpha_{\mathrm{o}} = 0$	43	13
	$S_{D_{\mathrm{i}}} = 0.5$	$\beta_{\mathrm{o}} = 0$		
	$S_{D_{\mathrm{o}}} = 0.5$			
Rocking scan (squares)	$S_{E_{\mathrm{i}}} = 0.1$			
	$S_{E_{\mathrm{o}}} = 0.1$	$\lvert\omega\rvert \leqslant 1.2$		
		$\alpha_{\mathrm{o}} = 0$	45	11
	$S_{D_{\mathrm{i}}} = 1$	$\beta_{\mathrm{o}} = 0$		
	$S_{D_{\mathrm{o}}} = 1$			
Diffuse scan out of the plane of incidence (triangles)	$S_{E_{\mathrm{i}}} = 0.1$	$\alpha_{\mathrm{i}} = 1.2$		
	$S_{E_{\mathrm{o}}} = 0.2$	$\beta_{\mathrm{i}} = 1.2$	43	13
	$S_{D_{\mathrm{i}}} = 0.5$	$\alpha_{\mathrm{o}} = 0$		
	$S_{D_{\mathrm{o}}} = 0.5$	$0 \leqslant \beta_{\mathrm{o}} \leqslant 8$		

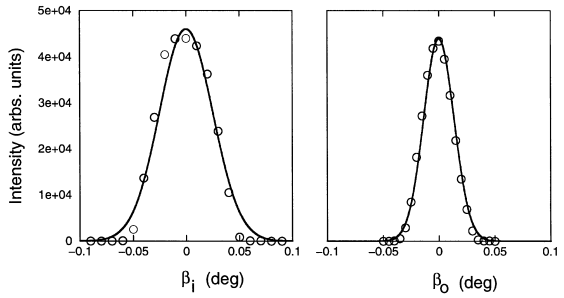

Fig. 2. Beam profiles used for the rocking scan and for the diffuse scan out of the plane of incidence displayed as circles and triangles, respectively, in Fig. 4. Experimental data (circles) and fits using Eq. (2) (solid lines). The resulting beam divergences from Eq. (3) are reported in Table 1 (row 1 and 3).

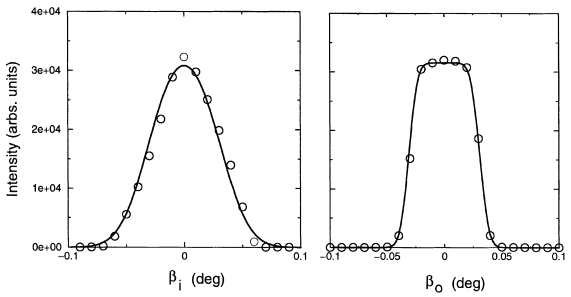

Fig. 3. Beam profiles used for the rocking scan displayed as circles in Fig. 4. Experimental data (circles) and fits using Eq. (2) (solid lines). The resulting beam divergences from Eq. (3) are reported in Table 1 (row 2).

To obtain the divergences $\Delta\alpha_{i,o}$ of the beam from the $\mathrm{HWHM}_{i,o}$ the contribution from the physical width (assumed to be Gaussian) must be removed:

$$\Delta\alpha_{i,o} = (\mathrm{HWHM}_{i,o}^2/(2\ln 2) - \arctan^2(S_{E_{i,o}}/D)/12)^{1/2}. \quad (3)$$

The values obtained for the horizontal and vertical divergences are reported in Table 1.

To study the off-specular diffuse scattering from our smectic film we performed scans out of the plane of incidence and rocking scans, respectively. In a rocking scan the angle $\omega = (\alpha_i - \beta_i)/2$ is varied, while $\theta = (\alpha_i + \beta_i)/2$ is kept constant. In the reciprocal space, q_x changes while q_z is effectively kept almost constant over the accessible range determined by the geometrical constraint $|\omega| \leqslant \theta$ imposed by the horizon of the sample. In this geometry $\boldsymbol{q}$ stays in the plane of incidence ($q_y = 0$, $\alpha_o = \beta_o = 0$). In a diffuse scan out of the plane of incidence the detector is moved by an angle β_o while $\alpha_o = 0$. To optimize the diffuse signal q_z was set at the first Bragg peak position corresponding to $\alpha_i = \beta_i = 1.2^0$. The detector scans the scattering parallel

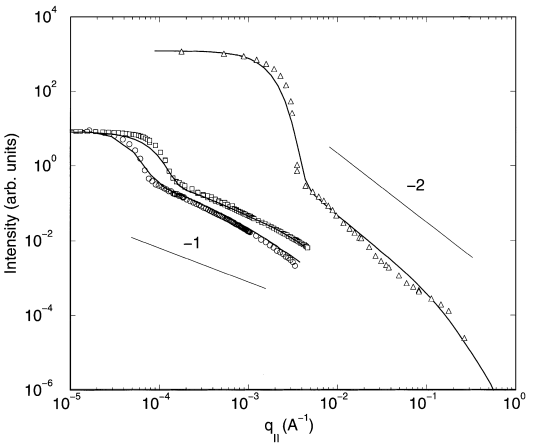

Fig. 4. Experimental scattering from free-standing smectic films. Diffuse scan out of the plane of incidence (triangles); rocking scan with detector slit $S_{D_o} = 1$ mm (squares); rocking scan with detector slit $S_{D_o} = 0.5$ mm (circles). Solid lines: fits to the data using the same physical parameters for the film $k_B T = 4.5 \times 10^{-21}$ J, $\gamma = 20 \times 10^{-3}$ N/m, elasticity modulus $K = 5 \times 10^{-12}$ N and compressibility modulus $B = 10^9$ N/m^2.

to the plane of the sample. In this way, q_y and q_x are probed over a very large and a small range, respectively, while q_z is kept constant on the specular ridge. The experimental values of the angles and the $\boldsymbol{q}$ range probed in each geometry are reported in Table 1. Note that the vertical divergence is much smaller than the horizontal one which makes the diffractometer particularly suitable for scans out of the plane of incidence. The results of the different scans are displayed in Fig. 4. All the data have been background subtracted and the geometrical asymmetry correction for rocking scans has been performed prior to analysis.

3. Resolution formalism

The experimental resolution accounts in the first place for the beam divergence, the solid angle defined by the detector finite aperture, and the wavelength dispersion. In other words, the wave vectors $\boldsymbol{k}_{in}$ and $\boldsymbol{k}_{out}$ are not ideally defined, but dispersed. The high monochromaticity of the beam allows to neglect the wavelength dispersion. The dispersion relative to $\boldsymbol{k}_{in}$ depends only on the divergences both horizontally and vertically, and is fully described by the mean square deviations $\Delta\alpha_{i,o}^2$. The dispersion relative to $\boldsymbol{k}_{out}$ stems only from geometrical considerations. It is due to the horizontal and vertical detector acceptance angles defined by both the detector slits and the illuminated area of the sample (footprint). Assuming Gaussian statistics, the mean square deviations describing the horizontal and vertical angular dispersions of the outgoing beam from the sample can be

shown to be equal to:

$$\Delta\beta_{i,o}^2 = \tfrac{1}{6}[(\beta_{i,o}^{min})^2 + (\beta_{i,o}^{max})^2], \quad (4)$$

where $\beta_{i,o}^{min}$ and $\beta_{i,o}^{max}$ correspond to the minimal and maximal detector acceptance angles in the horizontal and vertical plane, respectively. They depend on the full geometry of the experiment (scanning angle, footprint, slit sizes, distance D, beam divergence) [9]. Once these values are determined, $\mathscr{R}$ can be written directly as the Gaussian distribution function of all the angular random deviations [11]. In reciprocal space $\mathscr{R}$ can be written as a function of the joint-random deviation $\boldsymbol{q}'$ which are related to the independent angular deviations by $A = \langle q_i' q_j' \rangle$, the so-called covariance matrix. To use Eq. (1) one may resort to a simplified form using the eigenvalues of A which we denote as Δq_x^2, Δq_y^2 and Δq_z^2. In the corresponding eigenvector coordinate system of A, $\mathscr{R}$ reduces to [9]:

$$\mathscr{R}(\boldsymbol{q}') = \frac{(2\pi)^{-2/3}}{\Delta q_x \Delta q_y \Delta q_z} \exp\left(-\frac{1}{2}\frac{q_x'^2}{\Delta q_x^2}\right)\exp\left(-\frac{1}{2}\frac{q_y'^2}{\Delta q_y^2}\right) \times \exp\left(-\frac{1}{2}\frac{q_z'^2}{\Delta q_z^2}\right). \quad (5)$$

In our experiments, the eigenvector coordinate system differs not much from the original system. This is due to the fact that all the scanning angles stay within grazing incidence ($\lesssim 10^\circ$). Hence, we can use the following first order approximations for the resolution parameters in the rocking geometry [9]:

$$\Delta q_x^2 \approx k^2[\Delta\alpha_i^2 \Delta\beta_i^2 (\alpha_i + \beta_i)^2/(\Delta\alpha_i^2 + \Delta\beta_i^2)],$$
$$\Delta q_y^2 \approx k^2(\Delta\alpha_o^2 + \Delta\beta_o^2),$$
$$\Delta q_z^2 \approx k^2(\Delta\alpha_i^2 + \Delta\beta_i^2). \quad (6)$$

Note, however, that in the limit $\Delta\alpha_i \to 0$ the second-order must be taken into account leading to $\Delta q_x^2 \approx k^2(\alpha_i^2 \Delta\alpha_i^2 + \beta_i^2 \Delta\beta_i^2)^2/4$. For diffuse scans out of the plane of incidence and again in the limit of grazing angles, we can use the following first-order expressions [9]:

$$\Delta q_x^2 \approx k^2[4\alpha_i^2 \Delta\alpha_i^2 \Delta\beta_i^2/(\Delta\alpha_i^2 + \Delta\beta_i^2) + \beta_o^2 \Delta\alpha_o^2 \Delta\beta_o^2/(\beta_o^2 \Delta\beta_o^2 + \Delta\alpha_o^2 + \Delta\beta_o^2)],$$
$$\Delta q_y^2 \approx k^2(\Delta\alpha_o^2 + \Delta\beta_o^2),$$
$$\Delta q_z^2 \approx k^2(\Delta\alpha_i^2 + \Delta\beta_i^2). \quad (7)$$

4. Scattering formalism

Freely suspended smectic films are substrate-free weak scatters. Hence, the first Born approximation may serve to describe the reflected intensity. The scattering function can be written as [8,12]

$$S(\boldsymbol{q}) = R_F \int d\boldsymbol{r}_\parallel \exp(i\boldsymbol{q}_\parallel \cdot \boldsymbol{r}_\parallel) G(q_z, r_\parallel), \quad (8)$$

where $R_F \propto 1/q_z^4$ is the Fresnel reflectivity and $G(q_z, r_\parallel)$ is the height–height correlation function. For the simplified situation of conformally fluctuating incompressible films the latter can be written as

$$G(q_z, r_\parallel) = d\sum_{m,n}^{N} \exp\left[iq_z(m-n)d - \frac{1}{2} q_z^2 g(r_\parallel)\right], \quad (9)$$

with

$$g(r_\parallel) = \frac{k_B T}{2\pi\gamma}[\ln(r_\parallel/r_0) + K_0(r_\parallel/r_0) + c - \ln(2)].$$

In Eq. (9), $g(r_\parallel) = \langle [u(0) - u(r_\parallel)]^2 \rangle$, where $u(r_\parallel)$ represents the layers displacement along the (O_z) direction, K_0 is the modified Bessel function, $c \approx 0.5772$ Euler's constant, $r_0 = \sqrt{LK/(2\gamma)}$, with γ the surface tension, K the layer bending elasticity modulus, and $L = Nd$ the film thickness. Introduction of Eq. (8) together with Eq. (5) in Eq. (1) leads to:

$$I(\boldsymbol{q}) = \left[\int d^3 r G(q_z, r_\parallel) \exp(i(q_x x + q_y y) - \tfrac{1}{2}x^2 \Delta q_x^2 - \tfrac{1}{2}y^2 \Delta q_y^2)\right] \exp\left(-\frac{1}{2}\frac{q_z^2}{\Delta q_z^2}\right). \quad (10)$$

Note that because of the Landau–Peierls instability (see e.g. Refs. [13,14]) there is no correlation distance leading to an exponential decay of $G(q_z, r_\parallel)$. In smectic films G decays algebraically to zero and only the resolution factor can force the integral in Eq. (10) to converge.

5. Discussion

In Fig. 4 we report in addition to the experimental findings the results from the calculations of the scattering from our smectic film. The subscript $\parallel$ represents x in the case of rocking scans, and y for scans out of the plane of incidence. The results probed at low $q_\parallel$ range (left curves) correspond to rocking scans and the high $q_\parallel$ range (right curve) relates to a scan out of the plane of incidence. The same physical constants $k_B T = 4.5 \times 10^{-21}$ J, $\gamma = 20 \times 10^{-3}$ N/m [15] and $K = 5 \times 10^{-12}$ N [14] in accordance with literature, have been used to fit all the data. In addition, the calculations were done with the full correlation function instead of the approximated one given in Eq. (9), which also involves B, the compressibility modulus of the smectic layers [12]. We used the value $B = 10^9$ N/m^2 which is consistent with literature [8]. For the sake of clarity and because B does not influence much the $q_\parallel$-dependence of the intensity, we leave it out to describe the main features of the scattering patterns.

All the curves exhibit a large "plateau" region at low $q_\parallel$ followed by an abrupt fall-off at $q_\parallel \sim \Delta q_\parallel$ and a smooth negative slope at higher $q_\parallel$. The fall-off separates specular and off-specular dominated regions. This can be understood by geometrical considerations which show that $\Delta q_\parallel^2$ is the mean square value of the intensity distribution $I(q_z, q'_\parallel)$ collected by the detector when scanning around $q_\parallel = 0$. Around the center of this distribution, the detector aperture effectively collects the specularly reflected beam. The diffuse region is influenced both by the resolution and the correlation function, where the resolution depends on the specific geometry used. This leads to a further division into two parts. First, there is a region where the logarithmic term in $g(r_\parallel)$ is dominant (in between the "plateau" and high $q_\parallel$ regions). In this region, the intensity follows a law close to an algebraic decay of the form

$$I(q_\parallel) \sim \int \mathrm{d}\boldsymbol{r}_\parallel \exp(\mathrm{i}\boldsymbol{q}_\parallel \cdot \boldsymbol{r}_\parallel) r_\parallel^{-\eta} \sim q_\parallel^{-D+\eta}, \tag{11}$$

where $\eta = q_z^2 k_\mathrm{B} T/(4\pi\gamma) \approx 0.037$, and $D = 1$ or 2, depending on whether a one- or two-dimensional integration is performed. In Fig. 4, the diffuse scan out of the plane of incidence (right curve) follows a law according to $q_\parallel^{-2+\eta}$ as a result of the two-dimensional integration in Eq. (10). For the rocking scan with large $S_{D_\circ} = 1$ mm the integration over y has no effect and can be avoided in Eq. (10) [9]. This explains why the diffuse part behaves as $q_\parallel^{-1+\eta}$. In contrast, the other rocking curve with a smaller $S_{D_\circ} = 0.5$ mm shows a slope of -1.25 due to the necessary two-dimensional integration. This is different from the prediction above because $q_y = 0$ for rocking scans must be taken into account.

Finally, for values of $q_\parallel \gtrsim 10^{-1}$ Å^{-1} there is a nonlinear deviation from the algebraic decay. This higher-order effect is due to the bending elasticity modulus K in the correlation function. This can be well understood given the simplified development of $G(q_z, r_\parallel)$ in Eq. (9). Note that for the present choice of q_z at the first Bragg position the deviation can only be seen clearly in detector scans out of the plane of incidence.

6. Conclusion

We have described the influence of the resolution and related effects on the characteristic details of diffuse X-ray scattering patterns from free standing smectic films. We have used the general formalism developed in Ref. [9] to account for the experimental resolution and have applied it in the framework of the first Born approximation to analyze our data. Approximated relations for the main resolution parameters derived from the general formalism have been given for rocking scans and diffuse scans out of the plane of incidence. They give satisfying numerical results that account rather well for the three experimentally observed regions (specularly dominated part, algebraically decaying diffuse part, and elasticity dominated diffuse part).

Acknowledgements

This work is part of the research programme of the "Stichting voor Fundamenteel Onderzoek der Materie" (Foundation for the Fundamental Research of Matter, FOM) which is financially supported by the "Nederlandse Organisatie voor Wetenschappelijk Onderzoek" (Netherlands Organization for the Advancement of Research, NWO). DS acknowledges support from the TMR-Programme of the European Union (Contract ERBFMICT 9828877).

References

[1] M. Tolan, in: X-ray scattering from soft-matter thin films, Materials Science and Basic Research, Vol. 148, Springer, Berlin, 1999.
[2] V. Holy, U. Pietsch, T. Baumbach, High Resolution X-ray Scattering from Thin Films and Multilayers, Vol. 149, Springer, Berlin, 1999.
[3] J. Daillant, K. Quinn, C. Gourier, F. Rieutord, J. Chem. Soc. Faraday Trans. 92 (1996) 505.
[4] S.K. Sinha, M. Tolan, A. Gibaud, Phys. Rev. B 57 (1998) 2740.
[5] E. Vlieg, J. Appl. Cryst. 30 (1997) 532.
[6] A. Gibaud, G. Vignaud, S.K. Sinha, Acta Crystallogr. A 49 (1993) 642.
[7] W.H. de Jeu, J.D. Shindler, E.A.L. Mol, J. Appl. Crystallogr. 29 (1996) 511.
[8] E.A.L. Mol, J.D. Shindler, A.N. Shalaginov, W.H. de Jeu, Phys. Rev. E 54 (1996) 536.
[9] D. Sentenac, A.N. Shalaginov, A. Fera, W.H. de Jeu, J. Appl. Crystallogr. 33 (2000) 130.
[10] A. Fera, B.I. Ostrovskii, D. Sentenac, I. Samoilenko, W.H. de Jeu, Phys. Rev. E 60 (5) (1999) 5033.
[11] N.G. van Kampen, Stochastic Processes in Physics and Chemistry, North-Holland, Amsterdam, 1981.
[12] A.N. Shalaginov, V.P. Romanov, Phys. Rev. B 48 (1993) 1073.
[13] P.G. de Gennes, J. Prost, Physics of Liquid Crystals, Clarendon Press, Oxford, 1993.
[14] G. Vertogen, W.H. de Jeu, Thermotropic Liquid Crystals, Fundamentals, Springer, Berlin, 1988.
[15] P. Mach, C.C. Huang, T. Stoebe, E.D. Wedell, T. Nguyen, W.H. de Jeu, F. Guittard, J. Naciri, R. Shashidhar, N. Clark, I.M. Jiang, F.J. Kao, H. Liu, H. Nohira, Langmuir 14 (1998) 4330.